The AIMSS Project II: Dynamical-to-Stellar Mass Ratios Across the Star Cluster - Galaxy Divide

Duncan A. Forbes[1]⋆, Mark A. Norris[2], Jay Strader[3], Aaron J. Romanowsky[4,5],
Vincenzo Pota[1,5], Sheila J. Kannappan[6], Jean P. Brodie[5], Avon Huxor[7]

[1] *Centre for Astrophysics & Supercomputing, Swinburne University, Hawthorn VIC 3122, Australia*
[2] *Max Planck Institut fur Astronomie, Konigstuhl 17, D-69117, Heidelberg, Germany*
[3] *Department of Physics and Astronomy, Michigan State University, East Lansing, Michigan 48824, USA*
[4] *Department of Physics and Astronomy, San José State University, One Washington Square, San Jose, CA 95192, USA*
[5] *University of California Observatories, 1156 High Street, Santa Cruz, CA 95064, USA*
[6] *Department of Physics and Astronomy, UNC-Chapel Hill, CB3255, Phillips Hall, Chapel Hill, NC 27599, USA*
[7] *Astronomisches Rechen-Institut, Zentrum fur Astronomie der Universitat Heidelberg, Monchstrasse 12-14, D-69120 Heidelberg, Germany*

13 August 2014

ABSTRACT

The previously clear division between small galaxies and massive star clusters is now occupied by objects called ultra compact dwarfs (UCDs) and compact ellipticals (cEs). Here we combine a sample of UCDs and cEs with velocity dispersions from the AIMSS project with literature data to explore their dynamical-to-stellar mass ratios.

We confirm that the mass ratios of many UCDs in the stellar mass range 10^6 – 10^9 $M_\odot$ are systematically higher than those for globular clusters which have mass ratios near unity. However, at the very highest masses in our sample, i.e. 10^9 – 10^{10} $M_\odot$, we find that cE galaxies also have mass ratios of close to unity, indicating their central regions are mostly composed of stars.

Suggested explanations for the elevated mass ratios of UCDs have included a variable IMF, a central black hole, and the presence of dark matter. Here we present another possible explanation, i.e. tidal stripping. Under various assumptions, we find that the apparent variation in the mass ratio with stellar mass and stellar density can be qualitatively reproduced by published tidal stripping simulations of a dwarf elliptical galaxy. In the early stages of the stripping process the galaxy is unlikely to be in virial equilibrium. At late stages, the final remnant resembles the properties of $\sim 10^7$ $M_\odot$ UCDs. Finally, we discuss the need for more detailed realistic modelling of tidal stripping over a wider range of parameter space, and observations to further test the stripping hypothesis.

Key words: galaxies: dwarf – galaxies: star clusters – galaxies: evolution – galaxies: kinematics and dynamics

1 INTRODUCTION

The rate of discovery of new types of low mass stellar systems over the last 15 years has been remarkable. These new systems include Extended Clusters (ECs), Faint Fuzzies (FFs), Diffuse Star Clusters (DSCs) and Ultra Compact Dwarfs (UCDs). The latter have sizes and/or masses that approach those of dwarf ellipticals (dEs) and compact ellipticals (cEs). This discovery process usually begins with imaging that identifies candidates with *inferred* properties of size and luminosity that occupy a previously empty, or sparse, region of size-luminosity parameter space. The Hubble Space Telescope (HST), with its ability to partially resolve objects of size greater than 3 pc out to 40 Mpc distance, has played a key role. The next step is spectroscopic confirmation that the object is indeed associated with a larger host galaxy/group and is not merely a background object seen in projection. The scaling relation between physical size and luminosity of confirmed objects can then be examined, with the caveat that selection bias needs to be understood.

A further fundamental parameter of galaxies and star clusters alike is their internal velocity dispersion. Measuring

⋆ E-mail: dforbes@swin.edu.au

this usually requires dedicated spectroscopic follow-up with a high resolution spectrograph and long exposure times. As well as probing the velocity dispersion-luminosity scaling relation (i.e. extending the Faber-Jackson relation into the low mass regime), one can calculate dynamical mass and contrast it with stellar mass estimates to gain insight on issues such as the dark matter content and/or the stellar Initial Mass Function (IMF). After a few individual objects have been studied in this way, larger, and statistically-complete, samples of objects can eventually be examined.

As recently as 2007/8, the number of known cEs was only half a dozen (Chilingarian et al. 2007) and UCDs numbered around two dozen (Mieske et al. 2008; Dabringhausen et al. 2008; Forbes et al. 2008) with a largely empty gap in the parameter space of size-luminosity-velocity dispersion between them. This gap has been filled over the years (e.g. Chiboucas et al. 2011; Brodie et al. 2011; Forbes et al. 2013), but velocity dispersions for objects within the gap have not kept pace as they tend to be observed individually or in small numbers (Chilingarian & Mamon 2008; Price et al. 2009; Forbes et al. 2011; Penny et al. 2014).

Most recently, Norris et al. (2014; N14) has identified a number of UCD and cE candidates from HST archive imaging with a variety of telescopes used to confirm their distances. Velocity dispersions have been measured for over two dozen of them. Combining with the literature, a large number of confirmed objects now exist which fill the gap in velocity dispersion-luminosity parameter space between previously known UCDs and cEs.

In N14 we found many new objects to have lower stellar masses for a given velocity dispersion compared to dEs and normal elliptical galaxies. This is qualitatively consistent with UCDs and cEs being the tidally-stripped remnants of dEs and ellipticals, respectively (Bekki et al. 2003; Goerdt et al. 2008; Pfeffer & Baumgardt 2013; Faber 1973; Bender, Burstein & Faber 1992; Huxor et al. 2011). For example, the simulations of Pfeffer & Baumgardt (2013) placed a nucleated dE galaxy on various orbits in a Virgo cluster-like potential. After tidal stripping of the stars (there is no dark matter in their model) the final remnants have sizes and luminosities similar to those of observed UCDs and in some cases the remnants are so small that they resemble bright GCs (i.e. size $\sim$ 5 pc and $M_V \sim$ –9.5). Unfortunately they did not predict velocity dispersions. The objects discovered by N14 came from a range of environments including the field which is dominated by late type galaxies. Thus the progenitors of UCDs likely include disk galaxies with nuclei and/or bulges.

In N14 we also found evidence to support the idea of a gradual transition from in-situ formed old star clusters (globular clusters) to free-floating remnant nuclei or bulges, as one probes masses from 10^4 M$_\odot$ to 10^{10} M$_\odot$. UCDs in the mass range 10^6– 7×10^7 M$_\odot$ include both origins, but for masses $> 7 \times 10^7$ M$_\odot$ they are predominately remnants of stripped galaxies. We note that the transition is not only one of mass but also of size (Brodie et al. 2011; Forbes et al. 2013).

Previous observations of UCDs suggest that they have elevated dynamical-to-stellar mass ratios, and the ratio increases with object mass (e.g. Mieske et al. 2013 and references therein). Possible explanations, which may all be a consequence of an origin in tidal stripping, include the presence of central black holes, stars with a non-universal IMF and dark matter.

Central massive black holes are now known to be a common occurrence in large galaxies. Recently, Mieske et al. (2013) concluded that central black holes with a mass some 10-15 per cent of the current UCD mass could explain the elevated ratios. This is consistent with UCDs being the stripped remnants of $\sim$$10^9$ M$_\odot$ galaxy progenitors, based on the black hole–galaxy scaling relation.

The possibility of a different IMF in UCDs compared to globular clusters, with either bottom-heavy or top-heavy variants, has been suggested (Mieske et al. 2008). Recent support for a bottom-heavy IMF (more low mass stars) comes indirectly from observations of the cores of giant ellipticals (e.g. van Dokkum & Conroy 2010). In favour of a top-heavy IMF (more stellar remnants), Dabringhausen et al. (2012) recently showed that UCDs have low mass X-ray binary rates up to ten times those expected for a globular cluster-like IMF (but see also Phillips et al. 2013 for an alternative conclusion).

If tidal stripping has removed most of the initial galaxy's mass then the remnant will have a stellar population similar to that of the progenitor galaxy core. If this is the case, then the assumption of the same IMF for all UCDs gives a relatively lower stellar mass for the higher luminosity UCDs, thus effectively raising their apparent dynamical-to-stellar mass ratio.

Murray (2009) and Tollerud et al. (2011) have argued that if UCDs formed with a NFW-like dark matter profile (Navarro, Frenk & White 1997) then the expected dark matter density in the central regions would be some hundred times less than that observed for the stellar density, making dark matter relatively unimportant and unlikely to be the cause of the elevated ratios. Furthermore, Baumgardt & Mieske (2008) showed that any dark matter can be effectively 'pushed out' of a globular cluster even if it was present at formation. However, if UCDs formed from the tidal stripping of a larger galaxy, then the remnant UCD may still contain some of the progenitor's dark matter. For example, in the simulations by Goerdt et al. (2008) of the tidal stripping of a nucleated dwarf disk galaxy, gas that falls into the remnant core can effectively drag dark matter from larger radii into the core region. In the case of a gas-free progenitor dwarf elliptical galaxy the central regions of the remnant UCD would be expected to remain relatively dark matter free (Forbes et al. 2011). The search for dark matter in UCDs has the best chance of success in those UCDs with *low* stellar densities, i.e. low luminosity UCDs with large sizes (Willman & Strader 2012).

Mieske et al. (2013) recently carried out a study of UCDs in the Centaurus A group, and Fornax and Virgo clusters. In addition to reproducing the trend of a rising mass ratio with object mass, they claimed a bimodal structure in the mass ratio of the lower mass ($< 10^7$ M$_\odot$) UCDs. They suggested that this was consistent with the idea that low mass UCDs were a combination of stripped dwarf galaxies (with high mass ratios) and massive GCs (with low mass ratios). In this picture, only the high mass ($> 10^7$ M$_\odot$) UCDs reveal elevated ratios consistent with a pure stripping origin. With the enlarged UCD and cE dataset of N14, we will re-test the claims for a rising trend and bimodality in the mass ratios of UCDs. We also will address two key out-

Table 1. Physical properties of AIMSS compact stellar systems from Norris et al. (2014).

ID	M_V (mag)	R_e (pc)	σ_0 (km/s)	M_{dyn} ($M_\odot$)	M_* ($M_\odot$)	Ratio
NGC 0524-AIMSS1	-12.6	39.9±3.8	36.3±2.9	7.95±2.0 ×10^7	4.96±0.11 ×10^7	1.60±0.44
NGC 0703-AIMSS1	-15.0	164.7±28.4	20.1±7.0	1.01±0.87 ×10^8	3.13±0.98 ×10^8	0.32±0.38
NGC 0741-AIMSS1	-17.6	311.7±55.0	79.8±4.4	2.99±0.86 ×10^9	5.96±0.40 ×10^9	0.50±0.18
NGC 1128-AIMSS1	-15.6	76.0±10.9	76.9±7.0	6.79±2.2 ×10^8	7.50±0.16 ×10^8	0.90±0.31
NGC 1128-AIMSS2	-17.9	484.8±69.2	54.0±3.0	2.14±0.54 ×10^9	4.73±0.75 ×10^9	0.45±0.19
NGC 1132-UCD1	-14.8	84.3±12.1	93.5±9.5	1.11±0.39 ×10^9	3.28±0.88 ×10^8	3.40±2.09
NGC 1172-AIMSS1	-11.6	6.4±0.6	52.4±14.0	2.66±1.67 ×10^7	6.84±3.11 ×10^6	3.88±4.20
Perseus-UCD13	-12.8	88.6±8.6	38.0±9.0	1.93±1.10 ×10^8	2.72±1.10 ×10^7	7.10±6.92
NGC 2768-AIMSS1	-12.1	6.4±0.7	45.3±5.5	1.99±0.70 ×10^7	5.43±3.00 ×10^6	3.65±3.30
NGC 2832-AIMSS1	-14.9	46.4±6.7	133.7±13.2	1.25±0.43 ×10^9	2.37±0.86 ×10^8	5.28±3.72
NGC 3115-AIMSS1	-11.3	8.6±0.4	41.6±2.1	2.25±0.33 ×10^7	1.09±0.33 ×10^7	2.07±0.93
NGC 3923-UCD1	-12.4	12.3±0.3	43.4±2.8	3.50±0.54 ×10^7	1.97±0.56 ×10^7	1.77±0.77
NGC 3923-UCD2	-11.9	13.0±0.2	26.9±4.2	1.42±0.47 ×10^7	6.53±2.15 ×10^6	2.17±1.42
NGC 3923-UCD3	-11.3	14.1±0.2	19.0±4.4	7.69±3.67 ×10^6	2.37±0.80 ×10^6	3.24±2.64
NGC 4350-AIMSS1	-12.2	15.4±0.1	25.4±9.0	1.50±1.07 ×10^7	1.57±0.57 ×10^7	0.95±1.02
NGC 4546-UCD1	-12.9	25.5±1.3	20.0±2.3	1.54±0.43 ×10^7	3.59±0.86 ×10^7	0.42±0.21
NGC 4565-AIMSS1	-12.4	17.4±1.4	15.3±9.0	6.16±7.74 ×10^6	8.19±0.31 ×10^6	0.75±0.97
NGC 4621-AIMSS1	-11.9	10.2±0.4	41.9±5.4	2.71±0.80 ×10^7	1.64±0.38 ×10^7	1.65±0.87
M60-UCD1	-14.2	27.2±1.0	63.9±1.9	1.68±0.16 ×10^8	1.80±0.21 ×10^8	0.93±0.19
NGC 7014-AIMSS1	-15.2	329.8±23.6	19.0±5.8	1.80±1.22 ×10^8	2.99±0.98 ×10^8	0.60±0.60
UCD3/F-19	-13.5	86.5±6.2	26.6±4.9	9.25±4.07 ×10^7	4.96±1.15 ×10^7	1.87±1.25
NGC 2832-cE	-17.8	375.3±54.4	97.4±2.9	5.38±1.10 ×10^9	2.27±0.51 ×10^9	2.37±1.01
NGC 2892-AIMSS1	-18.9	580.9±85.0	137.5±3.7	1.66±0.33 ×10^{10}	1.09±0.12 ×10^{10}	1.53±0.47
NGC 3268-cE1	-15.9	299.9±21.9	33.3±13.6	5.03±4.47 ×10^8	1.30±0.26 ×10^8	3.86±4.20
Sombrero-UCD1	-12.3	14.7±1.4	39.5±3.6	3.47±0.96 ×10^7	1.64±0.41 ×10^7	2.11±1.11
M59cO	-13.4	35.2±1.2	25.7±2.2	3.19±0.66 ×10^7	7.49±0.11 ×10^7	0.42±0.09
ESO383-G076-AIMSS2	-17.4	652.2±57.5	97.5±8.9	9.37±2.53 ×10^9	2.60±0.53 ×10^9	3.59±1.70

Notes: Object name, V-band magnitude, stellar mass, effective radius and average uncertainties are from Norris et al. (2014). For central velocity dispersion see Section 2.1, and for dynamical mass see Section 4. Ratio is dynamical-to-stellar mass ratio, with the error calculated from the measurement uncertainties in velocity dispersion, effective radius and stellar mass. Objects in the lower part of the table are those that have been re-observed or are serendipitous.

standing issues relating to UCDs and cEs, namely 1) what is their origin? and 2) what is the cause of their elevated dynamical-to-stellar mass ratios?

In the next two sections we describe the new AIMSS data and additional data from the literaure. Section 4 describes our dynamical mass calculation. Section 5 discusses UCD formation via tidal stripping before presenting our results in Section 6. Our conclusions and thoughts on future work are given in Section 7.

2 THE AIMSS SAMPLE OF COMPACT STELLAR SYSTEMS

The Archive of Intermediate Mass Stellar Systems (AIMSS) targets compact stellar system candidates identified in the HST archive for spectroscopic followup (Norris & Kannappan 2011). The candidates are selected to have an inferred $M_V < -10$ and effective half light radius R_e that is twice the HST resolution limit of $0.1''$. Objects must also be relatively round ($\epsilon < 0.25$) and lie within 150 kpc in projection of a large galaxy ($M_V < -15$). No colour selection is applied. Objects with apparent magnitudes V < 21.5 are targetted for spectroscopic follow-up. Aperture velocity dispersion measurements are available for 27 objects in N14; 20 are new AIMSS objects and 7 are re-observed or serendipitous objects. For each object we list the V-band magnitude, total

stellar mass and effective radius from N14 in Table 1. To calculate stellar mass N14 used the code of Kannappan et al. (2013). This code uses the optical and infrared magnitudes, combined with a grid of stellar population models from Bruzual & Charlot (2003) covering ages from 5 My to 13.5 Gyr, and metallicities Z from 0.008 to 0.05 assuming a diet Salpeter IMF (which is similar to a Kroupa IMF for the purposes of calculating stellar masses). Had a normal, rather than diet, Salpeter IMF been adopted, the stellar masses would be systematically higher by ∼0.15 dex (and dynamical-to-stellar mass ratios lower). The effective radii come from fits to HST images of each object as determined by N14.

2.1 Calculating central velocity dispersions

The new velocity dispersion measurements presented in N14 are 'raw' in the sense that they are the value measured within the slit aperture quoted. The angular size of the objects of interest are on the same order as the slit, which is also comparable to our typical seeing. Thus in order to derive central velocity dispersions, we need to correct for light loss and the intrinsic surface brightness profile of the object. We use the aperture size, seeing and half light radius quoted in N14 and a King profile to make the corrections following method of Strader et al. (2011). When a Sersic

profile provides the best fit, we define the central velocity dispersion as the integrated value within $R_e/10$. Although these corrections are typically a few percent, the final dynamical mass depends on the corrected velocity dispersion squared. Our final central velocity dispersions and measurement uncertainties for the 27 AIMSS objects are included in Table 1.

3   LITERATURE DATA

As well as the objects listed in Table 1, we include various datasets from the literature.

In the Appendix Table A1, we list UCDs from the compilation of Mieske et al. (2013). They list *aperture* velocity dispersions in their table 3 for the bulk of these objects. In Table A1 we list the *central* velocity dispersions kindly supplied by Mieske & Baumgardt (2014, priv. comm.), supplemented by a few central values from Taylor et al. (2010). The errors quoted are measurement uncertainties only. The V-band magnitude, stellar mass and effective radius come from N14.

We exclude half a dozen Cen A objects from the original Mieske et al. (2013) list as they have $M_V > -10$. Although these objects could in principle be included in our analysis as GCs, we prefer to keep the GC sample homogeneous using only GCs from either the Milky Way or M31.

For other objects we take their properties, including their 'central' velocity dispersions, from N14. Briefly, we use Misgeld & Hilker (2011) and ATLAS^{3D} (Cappellari et al. 2011) for giant early-type galaxies, with dwarf ellipticals coming from Geha et al. (2002, 2003), Toloba et al. (2012) and Forbes et al. (2011). Local Group dwarf data are taken from Tollerud et al. (2013 and references therein). Compact ellipticals come from a variety of sources with the majority from Chilingarian et al. (2009) and Price et al. (2009). Milky Way GCs come from the compilation of Harris (2010) and M31 GCs from Strader et al. (2011). We note that N14 assumed all GCs to be uniformly old, which for a large sample of M31 and Milky Way GCs is a reasonable assumption. We do not consider young massive clusters (which are not old stellar populations) nor nuclear star clusters (for which very few velocity dispersions exist) in this work.

The size-stellar mass distribution for our entire sample is shown in Figure 1. Here we only show objects for which we have central velocity dispersions; for larger samples of objects with sizes and masses (or luminosities), but which lack velocity dispersions, see figure 13 of N14 (also Forbes et al. 2008; Brodie et al. 2011; Bruens & Kroupa 2012). Figure 1 shows objects traditionally classified as dwarf spheroidal (dSph), dwarf elliptical (dE), giant elliptical (gE), globular cluster (GC), ultra compact dwarf (UCD) and compact elliptical (cE), although the definition of such objects is often poorly defined and they can overlap in size-mass parameter space. For dSph, dE and gE galaxies we simply use their classification as defined by the literature sources listed above. Here we consider a GC to have stellar mass below 10^6 M$_\odot$. Such objects also have sizes $R_e < 10$ pc (a notable exception being the Milky Way GC NGC 2419 which is considered by some to be a UCD). We consider cEs to have stellar masses $> 10^9$ M$_\odot$ and $R_e < 800$ pc. UCDs are taken to have masses intermediate between those of GCs and cEs, irrespective of
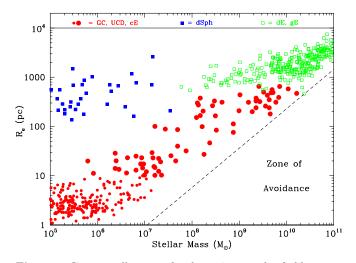

Figure 1. Size vs stellar mass for the entire sample of old, pressure supported systems with available central velocity dispersions. Blue squares denote Local Group dSph galaxies, and green open squares denote dE and gE galaxies. Red circles denote GCs, UCDs and cEs, with larger circles for objects with $R_e > 10$ pc. The diagonal dashed line demarks the constant surface density edge of the Zone of Avoidance, i.e. a high density region of parameter space that appears to be unoccupied. There is some overlap in size-mass parameter space between the traditional classification of different types of object.

their size (however we also the include the size of a UCD in our analysis below, e.g. many low mass UCDs have $R_e < 10$ pc). The Figure also shows the Zone of Avoidance, i.e. a high density region of parameter space that is so far largely unoccupied (see discussion in N14).

4   DYNAMICAL MASSES

Dynamical mass estimates for pressure-dominated systems can be obtained using the expression:

$$M_{\rm dyn} = C G^{-1} \sigma^2 R, \qquad (1)$$

where R is a measure of the size of the system and σ a measure of the system's velocity dispersion. Here we take the size of a system to be the effective radius (R_e) from N14, and the central velocity dispersion σ_0 from Table 1 for AIMSS objects, Table A1 for UCDs from Mieske et al. (2013) and Taylor et al. (2010), and N14 for all other objects. We note that using the central velocity dispersion over some scaled aperture, or a weighted global value, facilitates comparison with other pressure-supported systems.

To derive the dynamical mass one needs to know the virial coefficient C. A variety of approaches and hence values of C have been adopted in the literature, generally in the range $4 < C < 7.5$. Here we adopt $C = 6.5$ to be comparable to the dynamical mass calculations of Mieske et al. (2013). This value corresponds to a Sersic index of $n \sim 2$ (Bertin et al. 2002), which is a reasonable value for UCDs (Taylor et al. 2010) and for the objects that we focus on in this paper. Also, as shown later, such a value of C gives a mean dynamical-to-stellar mass ratio of close to unity for GCs (which are believed to be free of dark matter).

5 EFFECTS OF TIDAL STRIPPING

Before presenting our results, we briefly discuss the effects of tidal stripping on the properties of small galaxies (e.g. Forbes et al. 2003) as they are transformed into cEs and UCDs. Such a scenario is thought to be the dominant pathway for cEs and the more massive UCDs.

In general, tidal stripping will leave the central properties of a galaxy (e.g. velocity dispersion, metallicity, black hole mass) relatively unchanged. Here we are particularly interested in the effects of tidal stripping on the central velocity dispersion σ_0. In the seminal work by Bender, Burstein & Faber (1992) they noted that *...stripping of stars from the outer parts of a galaxy will leave σ_0 approximately constant....* Chilingarian et al. (2009) simulated the tidal stripping of a disk galaxy embedded within a dark matter halo of total mass $\sim 10^{12}$ M$_\odot$ within the potential of an M87-like galaxy. The final velocity dispersion of the remnant is within 10% of the original value even after $\sim$75% of the mass is stripped.

As mentioned in the Introduction, Pfeffer & Baumgardt (2013) simulated the tidal stripping of dwarf elliptical galaxies with nuclei on various orbits. Using a particle mesh code, they tracked changes of the stellar mass and size with time during the interaction but did not measure the velocity dispersion. The tidal stripping ('threshing') simulations of Bekki et al. (2003) did include velocity dispersion but they did not provide details of how of it evolved, simply noting that the *nucleus remains largely unaffected*. We expect σ_0 to be largely unchanged in the stripping process as the nuclei of dEs are relatively tightly bound.

Below we examine the evolution in dynamical-to-stellar mass ratio with time for two of the tidal stripping simulations of Pfeffer & Baumgardt (2013). In particular, we follow the 'stripping tracks' of a high mass (3×10^9 M$_\odot$) and low mass (7×10^8 M$_\odot$) dE progenitor, i.e. their simulations 39 and 3 respectively (with data kindly supplied by Baumgardt & Pfeffer 2014, priv. comm.). In the absence of a central velocity dispersion, we normalise the dynamical-to-stellar mass ratio to a value of unity at the start of each simulation (the model progenitors are dark matter free). At each time step, of 25 Myr, we recalculate the mass ratio (using the reduced size and stellar mass information from the simulations) until the end of the simulation (typically after a few Gyrs have elapsed). The final remnants have <1% of the mass of the progenitor, i.e. over 99% of the stellar mass has been lost due to stripping.

The key assumptions in this calculation are: 1) that the central velocity dispersion is unchanged; 2) that the virial coefficient is unchanged from the progenitor dE to the remnant; and 3) that the remnant is in virial equilibrium and hence equation 1 is valid. The first assumption appears to be valid to within $\sim$10% (20% in dynamical mass), and the second to within 40% (Bertin et al. 2002; Agnello et al. 2014).

6 RESULTS AND DISCUSSION

6.1 Comparison of dynamical and stellar masses

Recently, Mieske et al. (2013) re-examined the dynamical and stellar masses of CenA, Virgo and Fornax UCDs with well-measured properties. Before contrasting our re-
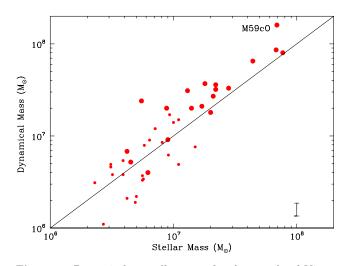

Figure 2. Dynamical vs stellar mass for the sample of Virgo, Fornax and CenA UCDs using data from Mieske et al. (2013). Larger circles denote objects with R$_e$ > 10 pc. The diagonal solid line shows a 1:1 relation. A typical observational error bar is shown lower right. The Mieske et al. sample shows that below about 10^7 M$_\odot$ UCDs scatter about the 1:1 relation, i.e. they are consistent with the total (dynamical) mass being due purely to stars. However, above this mass UCDs have systematically higher dynamical-to-stellar mass ratios. The larger-sized UCDs tend to also be those with the largest stellar masses. The massive UCD M59cO is labelled.

sults with theirs we first display their sample in Fig. 2. Rather than plot the dynamical-to-stellar mass ratio against mass (e.g. their figure 2), we prefer to plot dynamical vs stellar mass to avoid the possibility of any trend being dominated by simply the same quantity being plotted against itself (i.e. instead of A/B vs A we plot A vs B).

Figure 2 uses the dynamical and stellar masses directly from their table 3. Their dynamical mass calculations use a mass model and a profile tailored to each object. They note that in terms of the formula given by equation 1 above their approach is equivalent to a light profile with a virial coefficient $C \sim 6.5$. Their stellar masses are derived from each UCD's observed M$_V$ and [Fe/H] metallicity by applying a 13 Gyr, solar alpha abundance, single stellar population model (actually the mean of Maraston 2005 and Bruzual & Charlot 2003) with a Kroupa IMF.

The plot shows that the data scatter evenly about the unity relation for masses < 10^7 M$_\odot$. However, as noted by Mieske et al., the mass ratio for these objects is bimodal, almost avoiding ratios of unity. They found the distribution to be inconsistent with a unimodal distribution at the 99.2% level using the KMM test. Above 10^7 M$_\odot$ there is a tendency for the data to lie systematically above the unity relation (as also seen in figure 2 of Mieske et al. 2013). Figure 2 also shows that the high mass sample is dominated by objects with effective radii R$_e$ > 10 pc. The location of M59cO is highlighted; the Mieske et al. (2013) values suggest it has a large dynamical mass.

In Figure 3 we show our enlarged and revised sample of UCDs (i.e. combining Table 1 with other data from the literature). Dynamical masses are calculated using equation 1 using the R$_e$ values and central velocity dispersions as listed
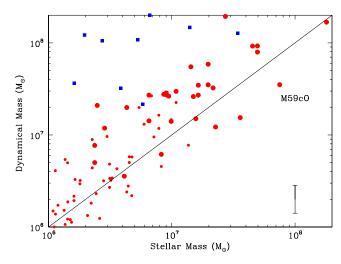
Figure 3. Dynamical vs stellar mass for the enlarged and revised sample of UCDs. Red circles denote UCDs, with larger circles for objects with $R_e > 10$ pc. Blue squares denote Local Group dSph galaxies. The diagonal solid line shows a 1:1 relation. A typical observational error bar is shown lower right. Excluding the dSph galaxies, our enlarged sample of UCDs shows the trend for elevated mass ratios as seen in the smaller Mieske et al. (2013) sample (Fig. 2), but does not support their claim for a bimodality in the mass ratios. The dynamical mass of M59cO is lower compared to the Mieske et al. sample due to the smaller velocity dispersion measured by N14.

Figure 4. Dynamical vs stellar mass for the enlarged sample of UCDs and GCs. Red circles denote GCs and UCDs, with larger circles for objects with $R_e > 10$ pc. Blue squares denote Local Group dSph galaxies. The diagonal solid line shows a 1:1 relation. Globular clusters, with stellar masses typically less than 10^6 M$_\odot$, scatter evenly about the 1:1 relation indicating that their total (dynamical) mass is consistent with their stellar mass.

in Table 1, with a virial coefficient for all objects assumed to be $C = 6.5$ (this includes the Local Group dSph galaxies shown in the figure). As well as a few UCDs with very high dynamical-to-stellar mass ratios (these are identified and discussed further in Section 6.2), the Figure reveals a few high mass UCDs now scattering below the unity relation. This includes M59cO with its dynamical mass based on our velocity dispersion of 25.7 ± 2.2 km s^{-1}. The dynamical mass of M59cO calculated by Mieske et al. (2013) is much higher as they used the literature value of 48 ± 5 km s^{-1} which N14 note was probably incorrect as it is close to the spectral resolution of the instrument used to obtain it (Chilingarian & Mamon 2008). This object illustrates how the quoted uncertainties in the literature are usually measurement uncertainties only and do not include systematic errors. An estimate of the latter can be seen in the scatter of the data points. With our enlarged and revised sample there is still a tendency for systematically higher mass ratios for the higher mass UCDs, confirming the trend seen in Figure 2. Figure 3 also shows that the transition to higher mass ratios for stellar masses of a few 10^6 to above 10^7 M$_\odot$ is very much driven by objects with $R_e > 10$ pc.

We do not see any strong evidence for the bimodal mass ratio trends claimed by Mieske et al. (2013). To illustrate this further, in Figure 4 we show a histogram of the dynamical-to-stellar mass ratios from Figures 2 and 3. As expected, the Mieske et al. (2013) data reveal a bimodal mass ratio distribution. Our enlarged sample does not, revealing a unimodal distribution peaked around unity. However, it should be noted that our sample includes objects more distant than the CenA, Fornax and Virgo objects of
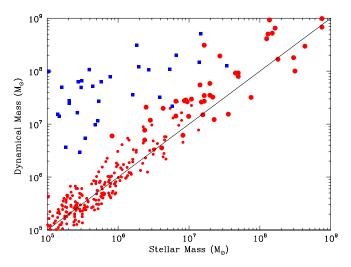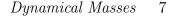
Mieske et al. and the resulting uncertainty in the dynamical masses is also greater (as indicated by the error bars in Figures 2 and 3). So although we do not see any evidence for the bimodality in the mass ratio of our low-mass UCDs, our uncertainties are higher than those in the Mieske et al. study and may have effectively washed-out a weak trend.

Next we extend the parameter space to smaller masses, to include objects traditionally called globular clusters (GCs), and to higher masses, but still excluding objects that might be considered compact ellipticals (i.e. with stellar masses $> 10^9$ M$_\odot$). Globular clusters are thought to be free of dark matter (and to lack massive central black holes) and so should have mass ratios that scatter about the unity relation. Using GC data for the Milky Way and M31 from N14, Fig. 5 shows that this is indeed the case. The trend, and level of scatter, are fairly similar from 10^5 to about 10^6 M$_\odot$. The level of scatter for the GCs ($\leqslant 0.3$ dex) gives an indication of the systematic errors in estimating dynamical-to-stellar mass ratios in this mass range. Systematic trends for M31 GC mass ratios with metallicity, which contribute to this scatter, are discussed in Strader et al. (2011).

Figure 6 extends the mass regime to include elliptical galaxies (i.e. cEs, dEs and gEs). A few caveats need to be kept in mind when interpreting this plot: 1) as we move from UCDs with Sersic n ~ 2 to gEs with n ~ 4, the virial coefficient should be reduced by $\sim 40\%$ to account for this change in structure, thus gradually reducing the dynamical mass (a downward change in Fig. 6 of ~ 0.15 dex); 2) the IMF may become more bottom-heavy in highest mass giant ellipticals (Conroy & van Dokkum 2012), which would increase stellar masses for a given luminosity (a rightward change in Fig. 6); 3) the samples of high mass UCDs and cEs are still incomplete (it is not clear if this incompleteness would affect the trends seen in Figure 6 or earlier Figures).

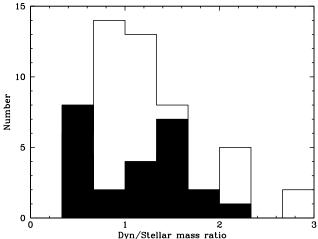In Fig. 6 we see that our sample reaches relatively high

Figure 5. Histogram of dynamical-to-stellar mass ratio for low-mass ($< 10^7$ $M_\odot$) UCDs. The Mieske et al. (2013) sample (from Figure 2), shown as a filled histogram, shows a bimodal nature to the mass ratios. However, our enlarged sample (from Figure 3), shown by an open histogram, does not.
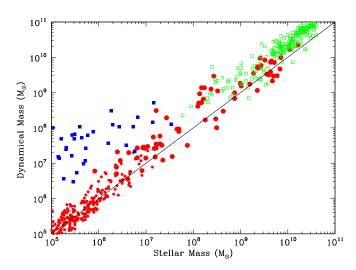

Figure 6. Dynamical vs stellar mass for the enlarged sample of GCs, UCDs, cEs and galaxies. Red circles denote GCs, UCDs and cEs, with larger circles for objects with $R_e > 10$ pc. Blue squares denote Local Group dSph galaxies, and green open squares denote dE and gE galaxies. The diagonal solid line shows a 1:1 relation. Although most UCDs/cEs with stellar masses around a few 10^8 $M_\odot$ show systematically elevated mass ratios, the ratio returns to near unity for the most massive UCDs/cEs.

masses of 10^{10} $M_\odot$ but remains fairly evenly scattered about the unity relation at the highest masses. The two cE galaxies with masses above 10^{10} $M_\odot$ come from Chilingarian et al. (2009). The figure also highlights the need to measure internal kinematics for more objects with stellar masses $\sim 10^8$ $M_\odot$ (e.g. Forbes et al. 2011).

Table 2. Mean dynamical-to-stellar mass ratios.

log M_* ($M_\odot$)	Mean Ratio	Median Ratio	Object Class
5–6	1.26 ± 0.07	1.04	GC
6–7	2.06 ± 0.27	1.33	UCD
7–8	2.98 ± 0.98	1.78	UCD
8–9	3.79 ± 0.78	3.40	UCD
9-10	1.48 ± 0.18	1.37	cE

6.2 Trends with Stellar Mass

To better visualise how the average mass ratio changes from GCs to cEs and to highlight any objects with extreme mass ratios, in Figure 7 we plot the mean dynamical-to-stellar mass ratio as a function of stellar mass. We include both AIMSS and literature samples. The plot shows half a dozen objects with extremely high mass ratios of 6–11, and a general locus of objects with lower mass ratios. First we discuss trends for the majority of objects and then focus on the extreme mass ratio objects.

The GCs have mass ratios close to unity as expected. For UCDs there is a consistent trend for increasing ratios up to a few 10^8 $M_\odot$ (albeit with large scatter). We also note a hint of a separate sequence of mass ratios around 3–4 in the stellar mass range $7 \times 10^5 < M_\odot < 7 \times 10^6$ for a dozen UCDs but this may be due simply to small number statistics. At the masses associated with cE galaxies ($> 10^9$ $M_\odot$), the mass ratio returns to being close to unity. Values for the mean mass ratios and the error on the mean, along with the median values, are given in Table 2. The median values, which are less effected by outliers, indicate a similar trend to the mean values.

Thus we do see some evidence of an upturn in the mass ratio above the mass limit of 7×10^7 $M_\odot$ as advocated by N14 at the transition to objects which are all formerly stripped galaxies. However, this ratio returns to unity for masses above 10^9 $M_\odot$, suggesting that the total mass of cE galaxies can be accounted for by their stars alone. We have estimated the effect of a changing virial coefficient for the mass range shown in Fig. 7 and find it is only a $\leqslant 40$ per cent effect, and therefore it cannot explain the observed trend. It is interesting that the mass ratio for cE galaxies is near unity, as cEs are generally thought to be the remnant of a larger galaxy (Faber 1973; Chilingarian et al. 2009; Huxor et al. 2011). Support for this view was also found by N14, in which we noted that most cEs have $\sigma_0 \sim 100$ km s^{-1}, typical for that of low mass ellipticals (whereas UCDs have $\sigma_0 \sim 45$ km s^{-1}, more typical of dwarf ellipticals).

As with our previous figures, the larger circles in Figure 7 indicate objects with $R_e > 10$ pc. As noted in the discussion of Figure 3, the transition to higher mass ratios as stellar mass increases from a few 10^6 to above 10^7 $M_\odot$ is very much driven by objects with $R_e > 10$ pc. All of the objects with apparent mass ratios above 5 have sizes $R_e > 10$ pc. We have investigated whether the mass ratio shows a continuous trend with the measured size for UCDs and cEs, and find none.

Figure 7 also shows the evolutionary 'stripping tracks' for two model galaxies from Pfeffer & Baumgardt (2013) as described in Section 5. The tracks have been normalised to
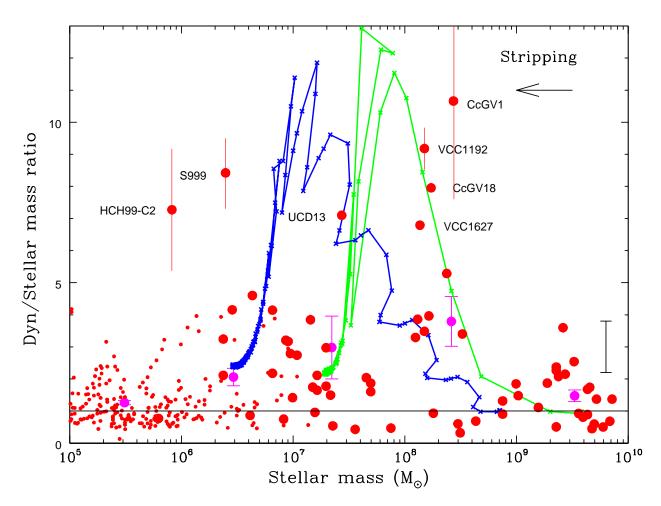
Figure 7. Dynamical-to-stellar mass ratio variation with stellar mass. Red circles show individual GCs, UCDs and cEs, with large circles for objects with $R_e > 10$ pc. Large magenta circles show the mean mass ratio (in bins of 1 dex) with errors on the mean. The solid black line shows the 1:1 relation of the mass ratio. The blue and green tracks show the effects of tidal stripping on the mass ratio in 25 Myr steps for two dE progenitors of different initial mass (the tracks have been normalised to a mass ratio of unity at the start of the simulation, with σ_0 assumed to be constant) from the models of Pfeffer & Baumgardt (2013). The arrow shows the general direction of stripping. Several high mass ratio objects, HCH99-C2, S999, CcGV1, CcGV18, VCC1192, VCC1627 and Perseus-UCD13 are labelled (with measurement error bars given for the four most extreme objects). A typical error bar for the whole sample is shown in the lower right. The data show a steady increase in the mean dynamical-to-stellar mass ratio from GCs (mass $< 10^6$ M$_\odot$) to those objects with stellar mass $\leqslant 10^9$ M$_\odot$, and then a decrease back to around unity for the highest mass cEs. The stripping tracks show that as stellar mass is lost from the progenitor dE galaxies, the inferred mass ratio increases in the first few hundred Myr and then decreases to a value similar to those of 10^7 M$_\odot$ UCDs.

a unity mass ratio at their initial (progenitor) mass. The stripping tracks show that as stellar mass is lost, the mass ratio first increases and then declines after several Gyr. The reason for this behaviour, is that instead of stellar mass and radius being reduced in lock-step, the simulations show that the initial stripping preferentially removes mass with little change in radius, while in the later stages the remnant becomes much smaller with limited mass loss.

It is likely that the extreme mass ratios inferred in the models at early stages in the stripping, and similar ratios calculated for some UCDs, indicate that the objects are out of virial equilibrium. In this sense, the mass ratio for both the simulation tracks and the observed objects should be considered to be an 'apparent' mass ratio and not a physical one. This is a short-lived early phase in the stripping process

– objects in this phase should be relatively rare and may reveal tidal features or extended halos in deep imaging. For example, VUCD7 is known to have a dual, core plus halo, structure. From a single Sersic fit its size is measured to be $R_e \sim 100$ pc (Evstigneeva et al. 2007) and we calculate an apparent mass ratio of $\sim$19 (not shown in Figure 7). However, if we were to use the core size of $R_e \sim 10$ pc and the stellar mass of the core, then its mass ratio would reduce to around 6. We note that our stellar population fit to the colours of VUCD7 are poor and therefore the dynamical-to-stellar mass ratio is uncertain. UCD13 in the Perseus cluster is another example of an object with a core plus halo surface brightness profile (Penny et al. 2014) and a relatively high inferred mass ratio from a single component fit (i.e. mass

ratio of 7). So in some cases, the high apparent mass ratios of UCDs are due to a dual-component structure.

A few of the objects with extreme apparent mass ratios are labelled in Figure 7. They include the CenA group UCD HCH99-C2 (Taylor et al. 2010), Virgo cluster UCD S999 (Hasegan et al. 2005), the Coma cluster cEs CcGV1 and CcGV18 (Price et al. 2009), Virgo cluster cEs VCC1192 and VCC1627 (Smith Castelli et al. 2013) and Perseus-UCD13 (Penny et al. 2014, and this work). Thus the measurements come from different literature sources and different instruments. For the four most extreme objects we show error bars which include the measurement uncertainty on R_e and σ_0, and we assume a magnitude uncertainty of ± 0.1 mag. The Figure shows that even taking into account measurement uncertainties these extreme objects have apparently elevated mass ratios. We have re-checked the transformation into stellar mass for these objects and find them to be reasonable. It is possible that some of these literature objects have an overestimated velocity dispersion, as was the case for M59cO, perhaps due to insufficient spectral resolution.

In summary, some of the extreme mass ratios for observed UCDs are due to a dual-component structure for which a single component fit gives rise to an inflated size measurement (e.g. VUCD7, Perseus-UCD13). Some objects may have spurious velocity dispersions in the literature (e.g. M59c0). For the remainder, it is unclear if measurements are in error or if the extreme apparent mass ratio is real. Deep imaging of these objects for extra-tidal features would be worthwhile.

It is worth emphasising that the apparent high mass ratios of the simulations only occur in the first Gyr. Thus it will be rare to catch a galaxy in this early stage of the stripping process.

At the final stages of the stripping process, after a few Gyr, the models have mass ratios and stellar masses consistent with 10^7 $M_\odot$ UCDs. We note that the mass ratio at the end of the simulation is ~ 2, as this simply reflects the the size-to-stellar mass ratio of the remnant to the progenitor. As the models are dark matter free, the final mass ratio should be unity. Thus our assumptions of a constant central velocity dispersion and/or virial coefficient may be incorrect. There may also be some resolution effects in the model itself, as at times during the stripping process the galaxy appears to briefly gain stellar mass. Nevertheless, the qualitative agreement between the tracks and the distribution of UCDs suggests that tidal stripping may be an alternative explanation for the elevated mass ratios and deserves further investigation.

6.3   Trends with Stellar Surface Density

Next we explore how the dynamical-to-stellar mass ratio varies with stellar surface density and what this may tell us about the cause of the rising mass ratio with object mass for UCDs. We calculate stellar surface density following N14, i.e. the stellar mass divided by the effective surface area of $2\pi R_e^2$.

In Figure 8 we show the mass ratio as a function of stellar surface density for UCDs and cEs only (i.e. we exclude GCs and other galaxy types). The plot includes the mean value and error on the mean (the median values, not shown, reveal a similar trend). The general trend is for the highest

density objects to have the lowest mass ratio, with the very highest density objects having mean mass ratios of unity. The half dozen UCDs and cEs with extreme mass ratios, and relatively low surface densities, are the same as labelled in Figure 7.

6.3.1   Dark Matter

The trend in Figure 8 is in the direction expected if an increased fraction of dark matter is responsible for the elevated ratios in UCDs. Although the density of baryons is so high in the highest stellar density UCDs that dark matter cannot be accommodated (Mieske et al. 2008), it may make a progressively larger contribution in the more diffuse objects. Detailed modelling is required to confirm this possibility.

6.3.2   Central Black Holes

According to Mieske et al. (2013), the elevated mass ratios for UCDs could be explained by central black holes that contribute 10-15 per cent of UCD masses. Most recently, strong evidence for a central black hole in a UCD has been reported from X-ray emission (Strader et al. 2013) and central velocities obtained by an integral field unit (IFU) with adaptive optics (Seth et al. 2014). The black hole represents 15 per cent of the mass of the UCD. Interestingly this object, named M60-UCD1, has a very high central density ($\sim 10^5$ $M_\odot$ pc^{-2}) but has a mass ratio close to unity (see Table 1). In this case, the velocity dispersion integrated within an aperture does not reveal the high velocities associated with a central black hole. It is also worth mentioning UCD3 in the Fornax cluster which has been observed with an IFU by Frank et al. (2011). They found no evidence for a black hole to within 5 per cent of the UCD mass. Clearly more UCDs require follow-up with the resolution sufficient to resolve the sphere of influence of the black hole.

Central black holes are the norm in high mass galaxies. If the trend seen in Figures 7 and 8 is due to the presence of black holes, then they must be preferentially dominating the dynamical mass (via the observed velocity dispersion) of the higher mass and lower density UCDs respectively. Larger relative contributions from the black hole would be expected in the systems that have been stripped of the most stars. It isn't obvious why this would be the case for the higher mass *and* lower density UCDs. Strangely, the cE galaxies, which are thought to come from higher mass progenitors than UCDs (and hence possess black holes), do not reveal elevated mass ratios.

6.3.3   Non-universal IMF

A non-universal IMF may give rise to the elevated mass ratios seen for UCDs. The IMF is observed to be more bottom-heavy in the cores of giant elliptical galaxies, revealing a strong trend with central velocity dispersion for $\sigma_0 \geqslant 200$ km s^{-1} (La Barbera et al. 2013; Ferreras et al. 2013; Conroy et al. 2013). The most massive ellipticals tend to have relatively low density cores, compared to lower mass ellipticals (Graham & Guzman 1993). Thus we might expect a trend for more bottom-heavy stellar populations in galaxies with lower central densities. A trend of this nature is seen
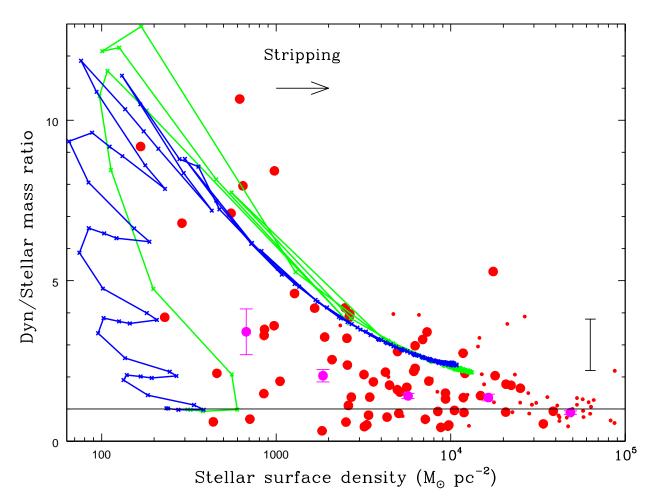
Figure 8. Dynamical-to-stellar mass ratio vs stellar surface density. Red circles show individual UCDs and cEs only, with larger circles for objects with $R_e > 10$ pc. Large magenta circles show the mean mass ratio (in bins of 0.5 dex) with errors on the mean. The solid black line shows the 1:1 relation of the mass ratio. A typical error bar for the whole sample is shown in the lower right. There is a general trend for decreasing mass ratios in the higher density systems. The blue and green tracks show the effects of tidal stripping on the mass ratio in 25 Myr steps for two dE progenitors (the tracks have been normalised to a mass ratio of unity at the start of the simulation, with σ_0 assumed to be constant) from the models of Pfeffer & Baumgardt (2013). The arrow shows the general direction of stripping. The stripping tracks show that the progenitors start with a relatively low average density but after a few hundred Myr the remnants become more dense as the nuclei increasingly dominate and the mass ratios get smaller as the stripping progresses.

in Figure 8, with UCDs and cEs having higher mass ratios at lower surface densities. However, all of the UCDs and cEs have $\sigma_0 < 200$ km s^{-1} and are therefore unlikely to be the remnant cores of giant ellipticals.

In the case of a top-heavy IMF, Dabringhausen et al. (2010) showed that high central densities (which promoted encounters between proto-stars) were associated with a top-heavy IMF. Assuming that the current stellar densities of UCDs reflect their initial central densities, then the trend seen in Figure 8 is the opposite of that expected for a top-heavy IMF.

6.3.4   Tidal Stripping

In Section 6.2 we suggested that tidal stripping was another possible reason for the elevated mass ratios of UCDs. The 'stripping tracks' of the same two model galaxies from Figure 7 are shown in Figure 8. The model galaxies start out at

relatively low stellar density, they quickly rise in apparent mass ratio with little change in stellar density. The simulations may not be in virial equilibrium during these early stages of rapid change. This may also be true for the objects with apparently extreme mass ratios (see Figure 7 for the identity of several such objects).

In the later stages of the stripping process the simulations decline in mass ratio and increase in density, with both models ending up with a mass ratio and density similar to that of the average UCD. This latter stage evolution is qualitatively similar to the trend seen in the mass ratio of UCDs and cEs.

In summary, the trend for higher dynamical-to-stellar mass ratios in lower surface density UCDs and cEs is qualitatively consistent with an increased contribution of dark matter, stellar populations with a top-heavy IMF and tidal stripping. It is less likely to be explained by a bottom-heavy

IMF or an increasing contribution of a central black hole (despite good evidence for a black hole in at least one UCD).

7 CONCLUSIONS AND FUTURE WORK

Here we present central velocity dispersions and dynamical masses for a sample of 27 UCDs and cEs recently discovered by the AIMSS survey. These data are combined with literature data to provide the largest sample of UCDs and cEs with internal kinematic measurements and dynamical masses. Such objects have properties that are intermediate between traditional star clusters and small galaxies. Using this expanded and revised sample, we re-examine the elevated dynamical-to-stellar mass ratios in UCDs.

Although the scatter is large, we confirm that the dynamical-to-stellar mass ratios of UCDs are systematically higher than for globular clusters. However, at the very highest masses in our sample, i.e. $\geqslant 10^9$ M$_\odot$, we find that cE galaxies have mass ratios close to unity consistent with being composed largely of stars. We also re-examine claims for a bimodal mass ratios among low-mass (i.e. less than 10^7 M$_\odot$) UCDs. Although we find no evidence to support this in our combined sample, our larger uncertainties may have 'washed-out' a weak trend.

In the literature various possible reasons for the elevated mass ratios in UCDs have been put forward. These include a variable IMF, a central massive black hole and the presence of dark matter. Here we present another possible reason for the elevated mass ratios, i.e. tidal stripping.

We find that the *final* stellar mass, stellar density and dynamical-to-stellar mass ratio of the tidally stripped dE progenitors in the simulations of Pfeffer & Baumgardt (2013) are in reasonable agreement with the typical observed values for UCDs (under the assumption that the central velocity dispersion and virial coefficient are largely unchanged in the process). However, at early stages in the stripping process, the galaxy is probably not in virial equilibrium. This may explain the apparent extreme dynamical-to-stellar mass ratios of up to 10 for some objects. We also note that some of the extreme mass ratio objects reveal dual-component structures and/or may have spurious measurements in the literature.

Despite some tantalizing results, there is a clear need for detailed realistic modelling of tidal stripping. Models need to be extended in mass to include higher mass progenitors (the likely progenitors of cE galaxies). As the morphology of the progenitor has an important effect on the efficiency of stripping and the structure of the remnant, a range of central densities needs to be explored. A range of orbits from circular to plunging radial orbits, within different gravitational potentials, should be modelled. The properties of the remnant that need to be predicted, in addition to size and luminosity (Pfeffer & Baumgardt 2013), include age, metallicity, colour, dark matter mass, and particularly the internal kinematics (e.g. central velocity dispersion) and the resulting dynamical mass.

On the observational side, confirming the presence of dark matter in UCDs will be very challenging. However, exploring the other possible explanations for the elevated mass ratios hold more promise. IMF variations in UCDs can be constrained by obtaining very high signal-to-noise spectra that include IMF sensitive features such as the NaI and Wing Ford bands at red wavelengths (van Dokkum & Conroy 2010). Adaptive optics observations of the cores of UCDs can be used to obtain the central velocity fields and hence search for the rapid motions associated with a massive black hole (Frank et al. 2011; Seth et al. 2014). If the stripping scenario is correct, we expect UCDs in the early stages of stripping to reveal the presence of extra-tidal features, such as halo structures or tidal tails.

8 ACKNOWLEDGEMENTS

9 REFERENCES

Agnello A., Evans N. W., Romanowsky A. J., 2014, arXiv, arXiv:1401.4462
Baumgardt, H., Miseke, S., 2008, MNRAS, 391, 942
Bekki K., Couch W. J., Drinkwater M. J., Shioya Y., 2003, MNRAS, 344, 399
Bender R., Burstein D., Faber S. M., 1992, ApJ, 399, 462
Bertin G., Ciotti L., Del Principe M., 2002, A&A, 386, 149
Brodie J. P., Romanowsky A. J., Strader J., Forbes D. A., 2011, AJ, 142, 199
Bruzual G., Charlot S., 2003, MNRAS, 344, 1000

Brüns R. C., Kroupa P., 2012, A&A, 547, A65

Cappellari M., et al., 2011, MNRAS, 413, 813

Chiboucas K., et al., 2011, ApJ, 737, 86

Chilingarian I., Cayatte V., Chemin L., Durret F., Laganá T. F., Adami C., Slezak E., 2007, A&A, 466, L21

Chilingarian I. V., Mamon G. A., 2008, MNRAS, 385, L83

Chilingarian I., Cayatte V., Revaz Y., Dodonov S., Durand D., Durret F., Micol A., Slezak E., 2009, Sci, 326, 1379

Conroy C., van Dokkum P. G., 2012, ApJ, 760, 71

Conroy C., Dutton A. A., Graves G. J., Mendel J. T., van Dokkum P. G., 2013, ApJ, 776, L26

Dabringhausen J., Hilker M., Kroupa P., 2008, MNRAS, 386, 864

Dabringhausen J., Kroupa P., Pflamm-Altenburg, J., Mieske, S., 2012, ApJ, 747, 72

Evstigneeva E. A., Gregg M. D., Drinkwater M. J., Hilker M., 2007, AJ, 133, 1722

Faber S. M., 1973, ApJ, 179, 423

Ferreras I., La Barbera F., de la Rosa I. G., Vazdekis A., de Carvalho R. R., Falcón-Barroso J., Ricciardelli E., 2013, MNRAS, 429, L15

Forbes D. A., Beasley M. A., Bekki K., Brodie J. P., Strader J., 2003, Sci, 301, 1217

Forbes D. A., Lasky P., Graham A. W., Spitler L., 2008, MNRAS, 389, 1924

Forbes D. A., Lasky P., Graham A. W., Spitler L., 2011, MNRAS, 415, 2976

Forbes D. A., Pota V., Usher C., Strader J., Romanowsky A. J., Brodie J. P., Arnold J. A., Spitler L. R., 2013, MNRAS, 435, L6

Frank M. J., Hilker M., Mieske S., Baumgardt H., Grebel E. K., Infante L., 2011, MNRAS, 414, L70

Geha M., Guhathakurta P., van der Marel R. P., 2002, AJ, 124, 3073

Geha M., Guhathakurta P., van der Marel R. P., 2003, AJ, 126, 1794

Goerdt T., Moore B., Kazantzidis S., Kaufmann T., Macciò A. V., Stadel J., 2008, MNRAS, 385, 2136

Graham A. W., Guzmán R., 2003, AJ, 125, 2936

Harris W. E., 2010, arXiv:1012.3224

Haşegan M., et al., 2005, ApJ, 627, 203

Kannappan S. J., et al., 2013, ApJ, 777, 42

La Barbera F., Ferreras I., Vazdekis A., de la Rosa I. G., de Carvalho R. R., Trevisan M., Falcón-Barroso J., Ricciardelli E., 2013, MNRAS, 433, 3017

Maraston C., 2005, MNRAS, 362, 799

Mieske S., Dabringhausen, J., Kroupa P., Hilker, M., Baumgardt, H., 2008, AN, 329, 964

Mieske S., et al., 2008, A&A, 487, 921

Mieske S., Frank M. J., Baumgardt H., Lützgendorf N., Neumayer N., Hilker M., 2013, A&A, 558, A14

Misgeld I., Hilker M., 2011, MNRAS, 414, 3699

Murray N., 2009, ApJ, 691, 946

Navarro J. F., Frenk C. S., White S. D. M., 1997, ApJ, 490, 493

Norris M. A., Kannappan S. J., 2011, MNRAS, 414, 739

Norris, M., et al. 2014, MNRAS, submitted

Penny S. J., Forbes D. A., Strader J., Usher C., Brodie J. P., Romanowsky A. J., 2014, MNRAS, 439, 3808

Pfeffer J., Baumgardt H., 2013, MNRAS, 433, 1997

Phillipps S., Young A. J., Drinkwater M. J., Gregg M. D., Karick A., 2013, MNRAS, 433, 1444

Price J., et al., 2009, MNRAS, 397, 1816

Seth, A., et al. 2014, Nature, submitted Smith Castelli A. V., González N. M., Faifer F. R., Forte J. C., 2013, ApJ, 772, 68

Strader J., Caldwell N., Seth A. C., 2011, AJ, 142, 8

Strader M. J., et al., 2013, ApJ, 775, L6

Taylor M. A., Puzia T. H., Harris G. L., Harris W. E., Kissler-Patig M., Hilker M., 2010, ApJ, 712, 1191

Tollerud E. J., Bullock J. S., Graves G. J., Wolf J., 2011, ApJ, 726, 108

Tollerud E. J., Geha M. C., Vargas L. C., Bullock J. S., 2013, ApJ, 768, 50

Toloba E., Boselli A., Peletier R. F., Falcón-Barroso J., van de Ven G., Gorgas J., 2012, A&A, 548, A78

van Dokkum P. G., Conroy C., 2010, Natur, 468, 940

Willman B., Strader J., 2012, AJ, 144, 76

10   APPENDIX

Table A1. Central velocity dispersion of ultra compact dwarfs from the literature.

ID	σ_0 (km/s)
UCD1	41.6±1.0
UCD6	28.0±1.0
UCD2/F-1	27.4±0.6
UCD28/F-5	31.9±1.0
F-34	19.0±1.5
UCD31/F-6	16.3±2.1
F-51	28.1±1.6
UCD33/F-7	14.4±1.6
UCD36/F-8	34.1±1.3
UCD39/F-9	34.5±1.6
F-11	28.9±1.0
F-17	34.1±1.4
F-53	18.8±1.8
UCD46/F-22	41.9±1.5
UCD4/F-24	35.1±1.0
UCD5	26.8±2.6
VUCD1	40.3±1.7
S999	26.2±1.3
H8005	10.8±1.9
S928	23.8±0.9
VUCD3/S547	55.2±1.5
S490	51.9±2.7
S417	36.2±1.5
VUCD4	28.1±2.0
S314	44.4±1.4
VUCD5	33.4±1.6
VUCD6	31.7±1.8
VUCD7	45.1±4.1
HGHH92-C29/GC0041	20.7±1.8
HGHH92-C11/GC0077	20.3±1.5
VHH81-C3	20.6±1.1
f2.GC61/GC0150	20.6±1.2
VHH81-C5	17.5±2.2
HCH99-C2/GC0171	18.8±3.0
HGHH92-C6	25.7±1.5
HCH99-C15/GC0213	33.4±5.9
HCH99-C18/GC0225	24.1±1.3
HGHH92-C17/GC0265	24.3±2.9
HGHH92-C21/GC0320	22.9±1.4
HGHH92-C22/GC0326	23.3±1.8
HGHH92-C23/GC0330	51.2±3.7
HGHH92-C7/GC0365	28.2±2.4

Notes: Object name (ordered by Fornax, Virgo and CenA objects), and central velocity dispersion from Mieske & Baumgardt (2014, priv. comm.) and Taylor et al. (2010).